Under consideration for publication in J. Fluid Mech.

Bifurcation and stability analysis of a jet in crossflow. Part 1: Onset of global instability at a low velocity ratio

MILOŠ ILAK, PHILIPP SCHLATTER, SHERVIN BAGHERI AND DAN S. HENNINGSON

Linné FLOW Centre, Department of Mechanics, Royal Institute of Technology (KTH), SE-10044 Stockholm, Sweden

(Received 9 May 2011)

We study direct numerical simulations (DNS) of a jet in crossflow at low values of the jet-to-crossflow velocity ratio R. We observe that, as the ratio R increases, the flow evolves from simple periodic vortex shedding (a limit cycle) to more complicated quasi-periodic behavior, before finally becoming turbulent, as seen in the simulation of Bagheri *et al.* (2009*b*). The first bifurcation is found to occur at $R = 0.675$, and the observed shedding of hairpin vortices is linked to a possible existence of a local absolute instability connected to the region of reversed flow immediately downstream of the jet. We focus on this first bifurcation, and find that a global linear stability analysis predicts well the frequency and initial growth rate of the nonlinear DNS simulation at $R = 0.675$, and that good qualitative predictions about the dynamics can still be made at slightly higher values of R where multiple unstable eigenmodes are present. In addition, we compute the adjoint global eigenmodes, and find that the overlap of the direct and the adjoint eigenmode, also known as a 'wavemaker', provides additional evidence that the source of the first instability indeed lies in the shear layer just downstream of the jet.

1. Introduction

The jet in crossflow is a flow of high practical relevance. Smoke and pollutant plumes, fuel injection and mixing, film cooling, etc., are just a few of the important applications of this flow. A large body of work has been dedicated to the study of jet in crossflow in recent decades. A review of the progress made in recent years is given by Karagozian (2010) and the references therein include the major works on the subject. A number of incompressible direct numerical simulations (DNS) or large-eddy simulations (LES) of jets in crossflow at different parameters have been performed by Yuan *et al.* (1999); Muppidi & Mahesh (2005, 2007); Schlatter *et al.* (2010); Muldoon & Acharya (2010); Salewski *et al.* (2008). A recent compressible DNS of a reactive fuel jet in crossflow was performed by Grout *et al.* (2010). Film cooling is another important application where more detailed knowledge of the dynamics of jets in crossflow is desired, and this flow regime has been studied using both experiments and simulations (Ziefle 2007; Jovanović 2006). Other experimental studies include Fric & Roshko (1994); Kelso *et al.* (1996); Smith & Mungal (1998); Lim *et al.* (2001); Megerian *et al.* (2007); Davitian *et al.* (2010). Theoretical work on the jet in crossflow includes Coelho & Hunt (1989); Alves *et al.* (2007, 2008); Cortelezzi & Karagozian (2001). Besides the obvious interest from an application point of view, the jet in crossflow puts to the test simulation capabilities and the various

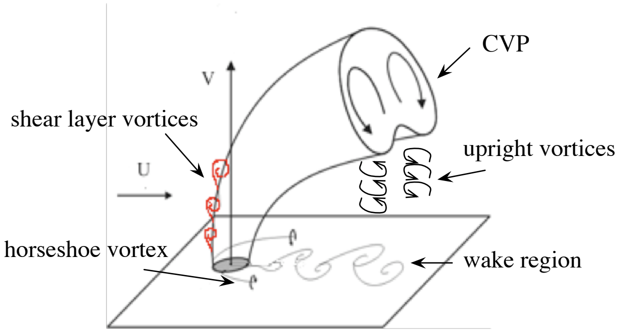

FIGURE 1. A schematic of the jet in crossflow, indicating the main vortical structures that may be identified in the flow typically.

methods for studying fluid flows, since it is fully three-dimensonal and the many features of its complex dynamics often do not yield themselves to investigation under simplifying assumptions that are applicable to simpler flows.

A number of characteristic flow structures has been observed in both experimental and numerical investigations of the jet in crossflow, and for a wide range of flow parameters. These relevant parameters for the jet in crossflow configuration include the Reynolds number (both of the jet inflow and the crossflow), the pipe inlet size and shape, and the velocity ratio R. The latter is the key parameter in most studies. While different definitions of R have been used (for example, in compressible flows it takes into account density), the definition used by Bagheri *et al.* (2009*b*) is used here, as this work presents further investigation of the same setup. We thus define R as

$$R = \frac{V}{U}, \tag{1.1}$$

the ratio of the *peak* inflow velocity V of the jet and the free-stream velocity of the cross-flow boundary layer U. Alternative definitions are based on mass flux (see, for example, Karagozian 2010). The features of the flow observed both by previous investigations and in our simulations include the horseshoe vortex that develops upstream of the jet orifice, the shear layer that develops as the jet enters the boundary layer, and the counter-rotating vortex pair (CVP), and they persist at a wide range of flow parameters. Some other features, such as wake vortices or upright vortices Schlatter *et al.* (2010), are not always visible. These vortical structures are shown schematically in Fig. 1, and also illustrated clearly in Fig. 1 of Fric & Roshko (1994). The CVP is the dominating feature of the flow, and considerable attention has been devoted to its study, and in particular its origin and its stability. The two shear layers that form from the circular shear layer as the jet emerges from the orifice have also been studied extensively. These two shear layers, which will be referred to as the upstream and downstream shear layer here, are the source of Kelvin-Helmholtz vortex roll-up frequently observed in jets in crossflow. We are concerned primarily with the donwstream shear layer in this work, since we find that its stability determines the first bifurcation of the flow in our setup.

The theory of linear hydrodynamic stability has been extensively developed over the past decades (Drazin & Reid 1981; Schmid & Henningson 2001; Schmid 2007). The availability of modern computing resources has led to the development of techniques for stability analysis of complex flows using the existing theory. In particular, the use of linear stability theory for *global* analysis of nonlinear two-dimensional (2D) and three-dimensional (3D) flows has become more widespread. The advantage of this approach is that the entire flow can be studied based on numerical simulations, without the typically very restrictive assumptions and approximations that characterize the earlier *local* approaches. In particular, the assumption of weakly non-parallel flow is not necessary anymore, which is important for spatially evolving flows like the jet in crossflow, where the velocity field has very strong variation in both streamwise and spanwise directions. Both local and global methods from stability theory have been used to study self-sustained oscillations and the instabilities that cause them. For details on local approaches for parallel flows and their extension to study self-sustained oscillations in non-parallel flows, the reader is referred to, for example, the review by Chomaz (2005) and the references therein. A recent study by Tammisola *et al.* (2011) offers a detailed comparison of results from linear stability theory and the corresponding nonlinear dynamics of a confined wake. Recent efforts on global stability analysis have been reviewed by Theofilis (2011).

In the context of jets in crossflow, in the experimental study of Megerian *et al.* (2007), it was found that as the velocity ratio R is decreased, probe data from the upstream (windward) shear layer indicates a self-sustained oscillation, i.e., a clear and distinct frequency peak is present in the flow without any external forcing, and a limit cycle is observed. This behavior was further investigated by the experiments of Davitian *et al.* (2010), where the limit cycles are studied in greater detail. Our findings from DNS show the same type of behavior. Evidence for self-sustained oscillation is also discussed by Schlatter *et al.* (2010).

In this work, we refer to the change in the behavior of the solution after a long time (i.e., after transients have decayed) from a stable flow field to a limit cycle depending on a flow parameter as a bifurcation. While this is not a completely formal definition, the onset of self-sustained oscillations in the flow field as the velocity ratio R is increased is the most important feature of the dynamics. We refer to this qualitative change as the 'first bifurcation' throughout this work. We do not attempt a precise characterization of the bifurcation using the tools of dynamical systems theory for this complex three-dimensional flow, but it will be shown that the jet in crossflow exhibits characteristic features of a Hopf bifurcation, which also describes the shedding past a cylinder in two dimensions, or the limit cycle of the one-dimensional (1D) nonlinear Ginzburg-Landau equation.

The studies of Bagheri *et al.* (2009*b*) and Schlatter *et al.* (2010) established that the jet in crossflow dynamics at $R = 3$ is dominated by an interplay of three common instability mechanisms, which are summarized in table 1: Kelvin-Helmholtz shear layer roll-up (A), an anti-symmetric instability of the counter-rotating vortex pair that appears to be of elliptic type (B), and a von Kármán type of instability near the wall (C). Mechanisms A and B are observed along the jet trajectory, i.e., they are associated with the CVP and the two shear layers. The instability of type C has a much lower associated frequency, and manifests itself via two-dimensional vortical structures in the horizontal plane that are shed and convected downstream near the wall. These three types of instability are further discussed in Bagheri (2010), from which table 1 is reproduced here with some modification. In this paper, we seek to describe the dynamics starting from simpler cases that are steady and thus stable, and observing the transition to unsteady flow as R is increased. The results of our simulations have allowed the addition of the last column in table 1; we have also been able to determine that, as R is increased, the order in which the three types of instability arise is B, A, and, finally, C. The three mechanisms are therefore re-ordered here. We note that the quantitative results reported here are particular to the set of parameters and numerical setup we use in this work. Nonetheless, we believe that this work provides very useful qualitative insight into the dynamics of jets in crossflow, which is its main goal. In this paper we focus on an analysis of the

Mode	Local Mechanism	Symmetry	Location	R
B	Kelvin-Helmholtz instability	Symmetric	Jet region	$R > 0.675$
A	Elliptic instability	Anti-symmetric	Jet & wake region	$R > 2.25$
C	von Kármán instability	Anti-symmetric	Wall region	$R > 2.5$

TABLE 1. The three instability mechanisms in a jet in crossflow identified by Bagheri (2010), re-ordered in order of appearance as the velocity ratio R is increased in direct numerical simulations.

symmetric Kelvin-Helmholtz instability (B), while a detailed analysis of mechanisms A and C is left for the second part.

While many investigations have considered the stability analysis of different features of the jet in crossflow independently (see, for example, Alves *et al.* 2007, 2008), to the best of the authors' knowledge no entirely global analysis exists at a set of parameters where the flow evolves from stable to globally unstable, i.e., the first bifurcation can be characterized unambiguously. The self-sustained oscillation that arises in our DNSs just above the first bifurcation can be connected to the oscillator/amplifier dynamics of the reversed flow region and the associated shear layer located in the near-field just downstream of the jet. In addition to a thorough examination of the DNS data, we are able to confirm our findings about the physical mechanism of the instability using a global linear stability analysis. While the first global linear stability analysis of a jet in crossflow by Bagheri *et al.* (2009*b*) provided valuable insight into the dynamics of the flow at $R = 3$, it was performed in a regime where multiple instability mechanisms are present at the same time. Our analysis at much lower R allows for a more complete description of the dynamics of the first instability, and, in addition, a more thorough evaluation of linear stability theory as a prediction tool for three-dimensional non-parallel and nonlinear flows. The stability analysis predicts the growth rate and frequency of the instability very accurately at a value of R just above the bifurcation, and still gives reasonable predictions for higher values of R. On the other hand, we find that the shape and spatial frequency of the modes are different from those of the hairpin vortices observed in the limit cycle. In addition, we compute the three-dimensional adjoint global eigenmodes for the jet in crossflow, and present, to the best of our knowledge, the first fully 3D computations of the overlap of the global modes and adjoint global eigenmodes, known as 'wavemaker' (Giannetti & Luchini 2007), which points to the core of the first instability and provides additional evidence in favor of the downstream shear layer instability.

This paper is organized as follows. Section 2 describes the numerical method and the simulation parameters used, as well as an overview of the DNS results. The first bifurcation is discussed detail in Section 3, and an explanation of the observed dynamics is proposed. In Section 4, we describe the global stability analysis performed in order to characterize the instability and the sensitivity analysis using global adjoint eigenmodes. Finally, a summary of the results and the conclusions that we draw from them are given in Section 5.

2. Direct numerical simulations of the jet in crossflow

2.1. *Computational setup*

The jet in crossflow is characterized by three independent dimensionless parameters†. For the present setup, the first is the Reynolds number $Re_{\delta_0^*} = U_\infty \delta_0^*/\nu$ based on the free-stream velocity of the boundary layer, U_∞, the boundary layer displacement thickness at the inflow, δ_0^*, and the kinematic viscosity ν, the jet Reynolds number based on the jet velocity and the jet diamater, $Re_{jet} = VD/\nu$, and the ratio of the jet velocity to the free-stream velocity, $R = V/U_\infty$. Alternatively, a Reynolds number based on the jet diameter may be defined as $Re_D = U_\infty D/\nu$, as, for example, in Kelso & Smits (1995), and then the velocity ratio is determined by $R = Re_{jet}/Re_D$. In this work $Re = 165$ and the jet diameter has a constant value of $D = 3$, so that R is the only parameter that changes. The jet nozzle center is at $x = 9.375$, where $\delta^* = 1.08$ which corresponds to $Re_{\delta^*} \approx 178$.

The jet in crossflow was simulated using SIMSON (Chevalier *et al.* 2007), a fully spectral, massively parallel DNS solver for the incompressible Navier-Stokes equations. The 2D parallelization described by Li (2009) enables the simulation to run on hundreds or thousands of CPUs. The jet inflow velocity profile is introduced on the wall as a Dirichlet boundary condition in a spatially developing Blasius boundary layer. The exact form of the profile corresponds to a laminar parabolic profile multiplied by a smoothing super-Gaussian function:

$$v(r) = R(1 - r^2)\exp(-(r/0.7)^4), \tag{2.1}$$

where v is the wall-normal velocity, R is the velocity ratio defined in Eq. 1.1, and r is the distance from the centre of the jet nozzle (x_{jet}, z_{jet}), defined as:

$$r = (2/D)\sqrt{(x - x_{jet})^2 + (z - z_{jet})^2}. \tag{2.2}$$

More details on this choice of profile are given in Bagheri *et al.* (2009*b*). While at low values of R some backflow into the jet pipe is to be expected under realistic conditions, it was demonstrated by (Schlatter *et al.* 2010) that most of the relevant physics is still captured by the simulations, especially far away from the jet orifice (such as the CVP). One feature that our simulations can not reproduce is the flow separation inside the pipe, which may play a significant role at low R. However, the qualitative similarity of our results to those of Ziefle (2007)(see next section) indicates that even in the regime considered here the characteristic dynamics is reproduced.

The resolution for the computations was $256 \times 201 \times 144$ spectral collocation points in the streamwise, wall-normal, and spanwise directions respectively, and the computational box dimensions were $L_x = 75$, $L_y = 20$, $L_z = 30$, in units of the displacement thickness at the start of the computational domain, δ_0^*. It should be noted that, due to a fringe that imposes periodicity in the streamwise direction, the useful streamwise length of the domain is $60\delta_0^*$. The initial velocity field in all simulations consisted of a spatially developing Blasius profile without the jet. In order to trigger jet instabilities quickly, random noise of low amplitude was superimposed onto the initial field at $t = 0$. The noise is fully three-dimensional and no symmetries are enforced. The boundary condition on the top of the box exactly corresponds to a decaying potential solution away from the wall. This boundary condition, as well as the fringe forcing, is described in detail in Chevalier *et al.* (2007).

† This fact is easily shown via the Buckingham π theorem, since there are five variables: U,V,ν,D and δ_0^*, and two dimensions (length and time).

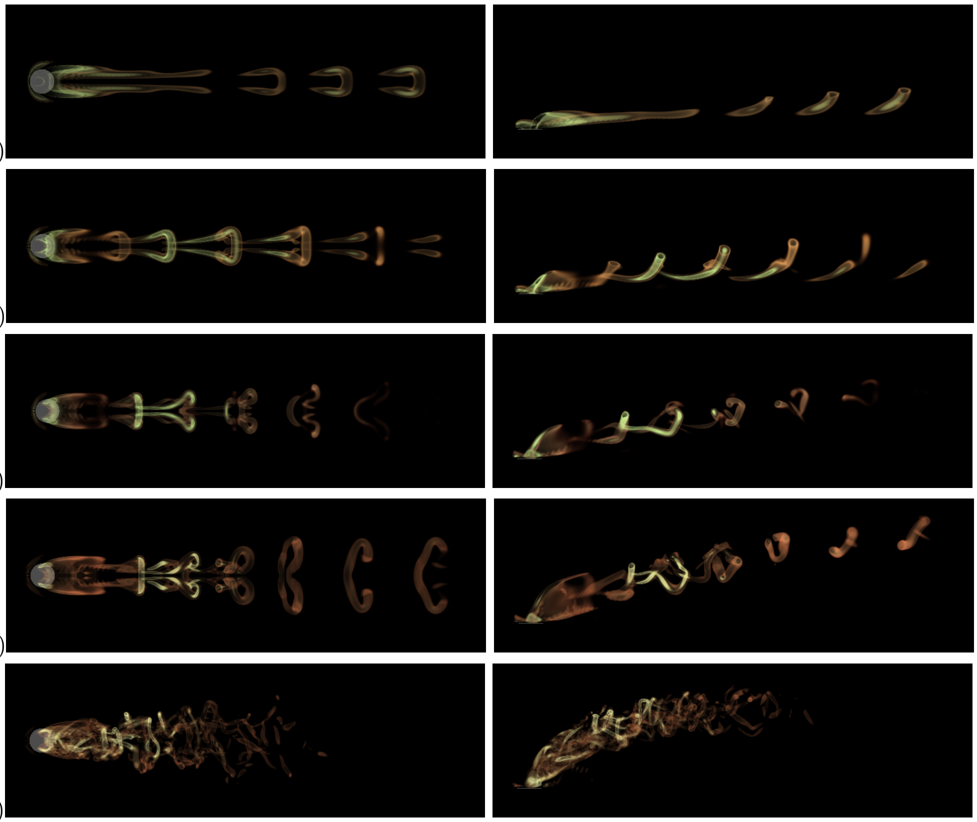

a)
b)
c)
d)
e)

FIGURE 2. Views from above (left) and side (right) views of the limit cycle for $R = 0.675$, $R = 1$, $R = 1.5$, $R = 2$ and $R = 3$(top to bottom). The snapshot of the $R = 3$ simulation is from the dataset of Schlatter *et al.* (2010).

2.2. *Direct numerical simulations*

The jet in crossflow was simulated for a range of R between 0.55 and 3. The simulations were ran for sufficiently long time for all transients due to the initial noise to decay. The dataset of (Bagheri *et al.* 2009*b*) at $R = 3$ was also included in this investigation. Snapshots from several of these runs are shown in Fig. 2, which shows top and side views of snapshots of selected DNS runs, visualized using volume rendering of the λ_2 vortex identification criterion (Jeong & Hussain 1995). Fig. 2 serves as a clear illustration of the 'roadmap' from a comparably simple jet structure to the turbulent jet in crossflow. Volume rendering allows insightful visualization of a flow field given appropriate choices of a colormap and an opacity transfer function. Animations of the runs shown in the figure can be seen in Ilak *et al.* (2010), where the full 3D dynamics of the vortex shedding is illustrated clearly. The colormap and the transfer function for the volume rendering in Fig. 2 were chosen so that the regions of highly negative value of λ_2 are colored in yellow (vortex 'cores'), and the regions of lower magnitude, i.e., negative value closer to zero, are colored in brown (vortex 'edges'), illustrating the vortical structures.

As Fig. 2 illustrates, as R is increased, the jet in crossflow goes through three regimes - stable flow that exhibits no unsteadiness, unstable flow where only shedding of spanwise-

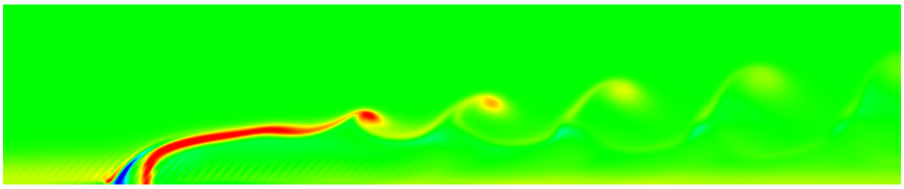

FIGURE 3. Spanwise vorticity for a snapshot of the run at $R = 1.0$, showing the windward (upstream) and leeward (downstream) shear layers. The downstream (leeward) shear layer is much stronger and sheds vortices due to a shear layer instability. Negative spanwise vorticity is shown in red, while positive spanwise vorticity is shown in blue.

symmetric hairpin vortices is present†, and, at $R > 2.25$, asymmetric flow that includes an interplay of both anti-symmetric and symmetric instabilities. In Fig. 2(a), at $R = 0.675$, simple and clearly defined hairpin vortices are visible, and as R increases through $R = 1$, $R = 1.5$ and $R = 2$ (Fig. 2(b),(c),(d)), the vortical structures become more complex, although the flow retains spanwise symmetry. A 2D cut in the spanwise symmetry plane ($z = 0$) at $R = 1$ is also illustrated in Fig. 3 for a cut in the spanwise symmetry plane, where the shedding of vortices from a strong shear layer downstream of the jet nozzle is observed. The vortex shedding is characteristic of a shear layer instability observed in two-dimensional flows, although the flow here is fully three-dimensional. Finally, as seen in Fig. 2(e), the flow at $R = 3$ is asymmetric and chaotic, characteristic of flow patterns typically observed in a jet. We emphasize again that both the jet inflow and the boundary layer crossflow are laminar, and the instabilities persist in the runs once they are excited. In this work, we will focus on the dynamics of the hairpin vortices, as illustrated in Fig. 2(a), and the instability mechanism that generates them.

An important factor in the development of the structures seen in the DNS simulations is the interaction of the jet and the crossflow boundary layer. This effect has been studied by Muppidi & Mahesh (2005), and it was found that the penetration of the jet into the crossflow depends on the boundary layer thickness at the nozzle position. The jet diameter, as one of the determining parameters, also plays a role in the jet penetration. In our work, both the boundary layer and the jet diameter are kept constant, and only R is varied. Thus, we are able to study the isolated effect of R. Trajectories of the jet for the different runs are plotted in Fig. 4 together with a line showing the thickness of the boundary layer δ_{99}, i.e., the line where the streamwise velocity of the corresponding Blasius solution is 99% of the freestream velocity. These trajectories were defined as in Muppidi & Mahesh (2005) — for each run, the trajectory was taken to be the streamline of the mean flow emanating from the center of the jet exit orifice. We see that for low values of R, the trajectory remains close to the edge of the boundary layer, which corresponds to the vortices being streched by the difference in streamwise velocity between the 'heads' and 'legs' of the hairpins, as opposed to the vortical structures seen at higher R, which are convected downstream in a region without external shear as soon as they leave the near-field region of the jet. It is interesting to note that in Fig. 4 (b), the trajectories appear to collapse well when both x and y are re-scaled by the product RD, which is not the case for higher values of R and the varying conditions studied by Muppidi & Mahesh (2005).

† Spanwise symmetry is defined here as u and v velocity components being symmetric about the $z = 0$ plane, and the w-component being anti-symmetric.

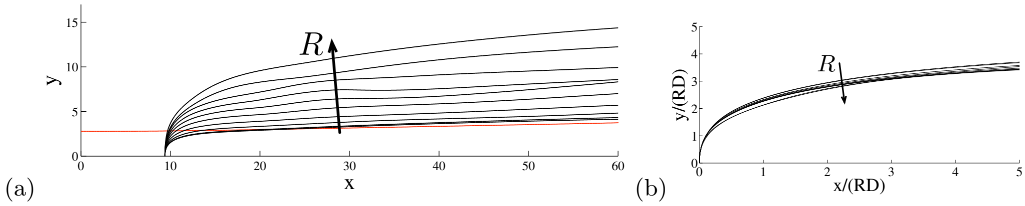

FIGURE 4. (a) Jet trajectories at different R. The red line corresponds to 99% of the freestream velocity. (b) Trajectories re-scaled by RD.

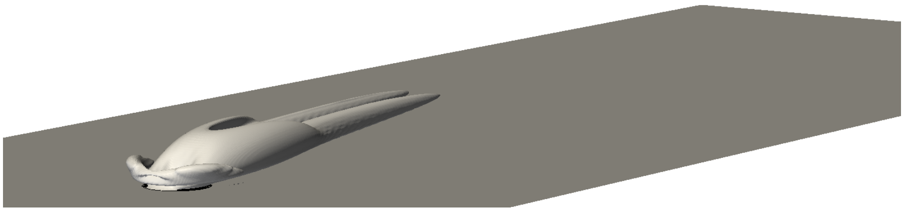

FIGURE 5. An isosurface of λ_2 for the steady case of $R = 0.65$. Hairpin vortices that are observed as transient features due to the initial noise have decayed in this case.

3. The first bifurcation

From now on, we focus on very low values of R, in particular, $R < 1$. In this section, we describe the first bifurcation and the proposed explanation of the dynamics at low R. A detailed analysis of the set of nonlinear DNS mentioned in the previous section will be reported separately in the second part of this work.

3.1. *Steady flow below R=0.675*

Since both the jet inflow and the boundary layer into which it is injected are laminar, our problem setup allows for a steady flow at values of R between 0.55 and 0.65. Therefore, apart from effects of numerical truncation, there are no disturbances or forcing after the asymmetric noise imposed initially has decayed. We observe hairpin vortices as transient features that may persist for a very long time, especially as R approaches $R = 0.675$, but eventually decay, resulting in a stable and steady vortex system shown in Fig. 5. This steady flow exhibits most of the features observed in jets in crossflow - a so-called horseshoe vortex is observed upstream of the orifice, a weak counter-rotating vortex pair (CVP) is dominating the flow downstream, and shear layers upstream and downstream of the jet orifice are present too. These two shear layers merge into an 'envelope' around the CVP. These features have also been observed and discussed by Bagheri *et al.* (2009*b*) when considering the artificially stabilized steady flow at $R = 3$, although we note here that the so-called secondary CVP (Schlatter *et al.* 2010) is not visible in this case, since the jet is very close to the plate. The steady CVP for this case does not extend nearly as far downstream as in the case of the unstable steady-state solution at $R = 3$ in Bagheri *et al.* (2009*b*), which is dominated by a very strong CVP. The fact that we observe a stable vortex system at very low R indicates that the unsteady shedding characteristic for jets in crossflow at higher R arises through a bifurcation, which is our primary interest in this work.

3.2. *Shedding of hairpin vortices at R=0.675*

At $R = 0.675$, the shedding of hairpin vortices is not a transient feature anymore, but a limit cycle develops instead. This case is of greatest interest for characterization of the instability mechanism, since it may be thought of as a 3D equivalent of, for example, a 2D cylinder in crossflow just above the critical Reynolds number. Side and top views of a snapshot of the limit cycle for this case are shown in Figure 2(a). In addition, two other three-dimensional views of a snapshot of the simulation are shown in Fig 6. Based on inspection of the λ_2 field seen in Fig 6(a), the hairpin vortices appear to form from the leeward shear layer and are continuously shed downstream. The legs of the vortices appear to form through merging of patches of vorticity from the downstream end of the CVP and the spanwise vortices shed from the shear layer. The streamwise spatial separation of the hairpin vortices is about 8.25 units; three such hairpin vortices fit into the computational box. This vortex shedding pattern corresponds to a self-sustained oscillation that also occurs in the flow past a cylinder, although the flow structures and the symmetry of the flow are different in the case of the jet. The change of the dynamics from a stable equilibrium to a limit cycle is characteristic of a Hopf bifurcation. This type of bifurcaton is often encountered in self-sustained oscillations of fluid flows, the 1D Ginzburg-Landau equation being a commonly studied example. Evidence for self-sustained oscillations in the jet in crossflow has been discussed in detail in Schlatter *et al.* (2010), as well as by Megerian *et al.* (2007), and will be described further towards the end of this section. Figure 6(b) shows the boundary of the reversed flow region (white) and the negative spanwise vorticity (dark grey) for the same snapshot of the DNS. The region of high negative spanwise vorticity corresponds to a strong shear between the reversed flow (backflow) region and the jet fluid. The formation and evolution of hairpin vortices has been described in detail by the landmark studies of Acarlar & Smith (1987a,b), where it was shown that these vortices arise as a result of roll-up of shear layers associated with regions of slowly moving fluid within a flow that is overall faster. Such shear layers also arise in the presence of reversed flow, as is the case for the jet in crossflow.

The hairpin vortices that we observe are remarkably similar to the ones observed by Ziefle (2007) for a Large Eddy Simulation (LES) of a compressible jet in crossflow, where the crossflow is steady and is taken to be the mean of a turbulent velocity profile. We note that the inflow pipe and a plenum are also carefully modeled in that simulation. We thus observe the correct vortex shedding mechanism even with a much simplified setup. The vortex shedding we observe is essentially the same as that observed in recent simulations at our parameters that include the pipe using a spectral element method†. The structures observed in the DNS runs at the low values of R also resemble very much those shown by Perry & Lim (1978), although no bouyancy effects are present in our simulations. The first instability of the jet in crossflow thus corresponds to a well-known phenomenon that has been observed and described in many other situations. It is the addition of more instabilities and physical mechanisms at higher R that make the jet the complex flow it is.

The wall-normal velocity signal from a probe in the region far downstream of the nozzle is shown in Fig. 7 (a), indicating that an oscillation at a constant frequency is established after a few hundred time units, with the amplitude of the limit cycle slowly growing until saturation. The location of this probe is indicated in Fig. 6(a) with a black dot. On the other hand, the velocity in the region right behind the jet remains constant (and negative, since the probe is in the reversed flow region seen in Fig. 6 (b)) after approximately one flow-through time, which is the time needed for the transients from the initial noise to

† Dr. Paul Fischer, Argonne National Laboratory, private communication

(a)

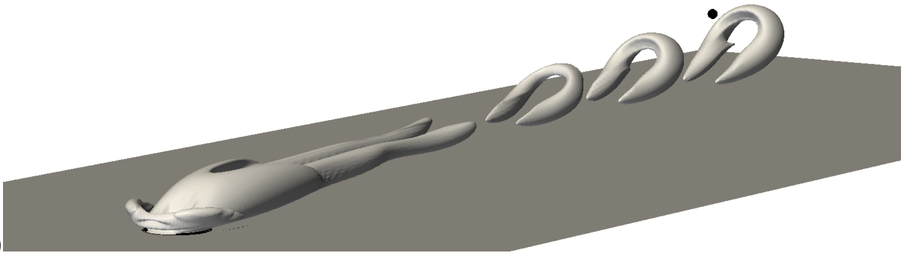

(b)

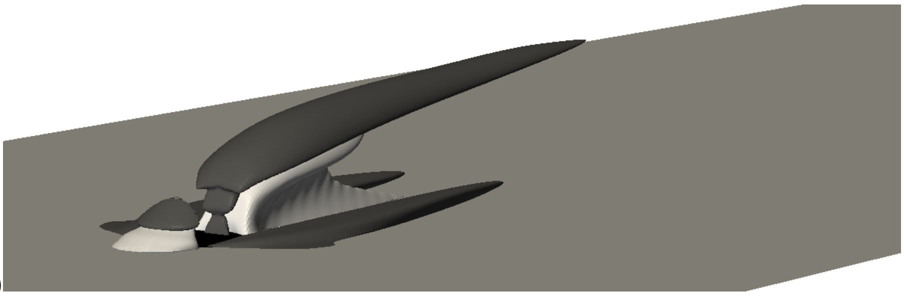

FIGURE 6. (a) A contour plot of the λ_2 criterion for a snapshot of the limit cycle of the simulation at $R = 0.675$. The black dot indicates the location of the velocity probe whose PSD is plotted in Fig. 7a. (b) The negative spanwise vorticity (dark grey) and the region of reversed flow (white) for the same snapshot are shown, indicating the location of the three-dimensional shear layer.

decay. There is no low-frequency oscillation associated with the reversed flow such as that observed by Bagheri *et al.* (2009*b*) at $R = 3$. The Power Spectrum Density (PSD) curve for the probe in Fig. 7 (a) is shown in Fig. 7 (c), the time series for the PSD being taken starting with $t = 1600$. A dimensionless frequency, or Strouhal number, for the jet in crossflow may be defined as:

$$St = \frac{fD}{V_{jet}}, \tag{3.1}$$

The Strouhal number for the DNS runs considered in this and the next section was found to decrease from 0.35 at $R = 0.675$ to 0.32 at $R = 0.8$.

3.3. *The dynamics of the self-sustained oscillation*

Self-sustained oscillation is defined as persistent oscillation of a system at a characteristic frequency without any forcing, or with small-amplitude forcing whose frequency is different that the one with which the system oscillates. A typical example is vortex shedding past a circular cylinder. Evidence has been presented in numerous works that self-sustained oscillations are related to the existence of a global instability, which corresponds to the existence of a localized source of instability waves, known as an *absolutely unstable region*. On the other hand, a flow may be convectively unstable, which means that instabilities are amplified as they are convected downstream, but the flow remains steady if no new disturbances continuously enter the domain upstream. Pockets of absolute instability are typically followed by convectively unstable regions downstream in flows that exhibit self-sustained oscillation. For a detailed treatment of absolute and convective instabilities and their relation to self-sustained oscillations, the reader is referred to, for example, Huerre & Monkewitz (1990), and the references therein, or the more recent review by Chomaz (2005).

The connection between self-sustained oscillations and the presence of reversed flow

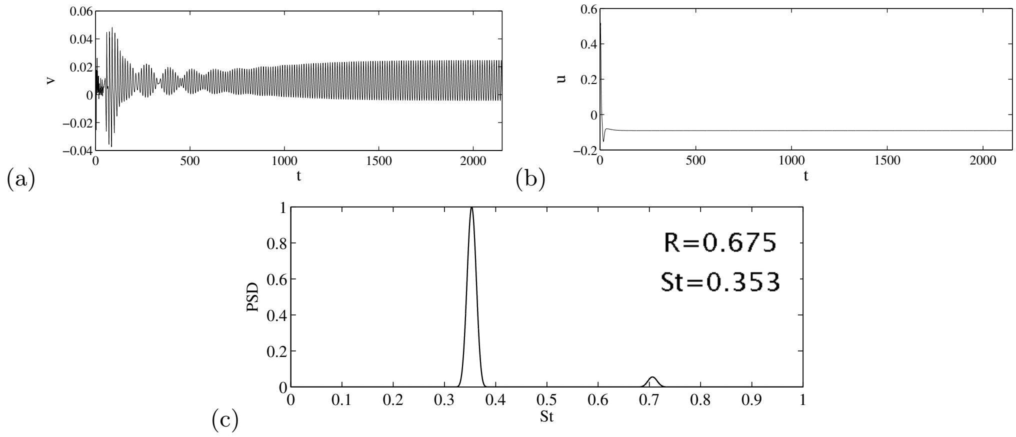

FIGURE 7. (a) Velocity probe of wall-normal velocity at $(50, 5.5, 1.5)$. The location of the probe is indicated with a black dot in Fig. 6(a). (b) A probe measuring streamwise velocity at $(11.7, 1.0.0.0)$, indicating that the flow is steady in the near-field of the jet. PSD of the probe in (a) computed starting with $t = 1600$, which indicates a strong peak at $St = 0.35$ and a lower peak at the first harmonic.

(backflow) regions in the context of the jet in crossflow was postulated by Schlatter *et al.* (2010). Since the jet acts as an obstacle to the crossflow, similarly to a solid cylinder, a region of reversed flow is formed immediately downstream of the jet, in which the streamwise velocity is negative. Using our simulation data at low R, we are in the position to examine this claim more closely. In the so-called oscillator/amplifier model, a localized region in the flow continuously sheds vorticity, which is then convected downstream by a convectively unstable region before decaying in the far field. A study of the stability of simple separation bubbles in 2D was undertaken by Hammond & Redekopp (1998), and it was shown that, for high enough magnitude of the reversed streamwise velocity, local absolute instabilities may be observed. These authors propose that the self-sustained oscillation arises from an absolutely unstable region of the flow near the peak of the negative streamwise velocity. Since a separation region is also present in the jet in crossflow, we examine it more closely for evidence that would support the oscillator/amplifier model where the oscillator is located in the region of sreversed flow.

Keeping in mind that the flow we are investigating is three-dimensional, and strongly non-parallel in both streamwise and spanwise direction, we take a closer look at the reversed region of the mean flow at values of R between 0.65 and 0.8†. A plane view of the separation region in the midplane ($z = 0$) is shown in Fig. 8 (a). At $R = 0.675$, the lowest value of the streamwise velocity is located in the $z = 0$ plane close to the wall ($y \approx 1.35$) at $x = 12.3$. The wall-normal profile at that point is shown in Fig. 8 (b) for different values of R. In Fig. 8 (c), the streamwise velocity profile at $z = 0$ is plotted for a number of stations in the streamwise direction, indicating the strength of the downstream shear layer in the near field of the jet, which appears to be susceptible to a possible local absolute instability that would be the source of the observed self-sustained oscillation. We note that a negative velocity is not necessarily required for instability, it is rather the stronger shear due to the reverse flow that would be more sensitive to perturbations.

A pocket of absolute instability may be sought through a local stability analysis — for

† A region of reversed flow just upstream of the jet exit related to the hovering vortex upstream of the nozzle is also visible in Fig. 8 (a). The shear layer associated with that region of the flow was found to be stable in all simulations considered in this work.

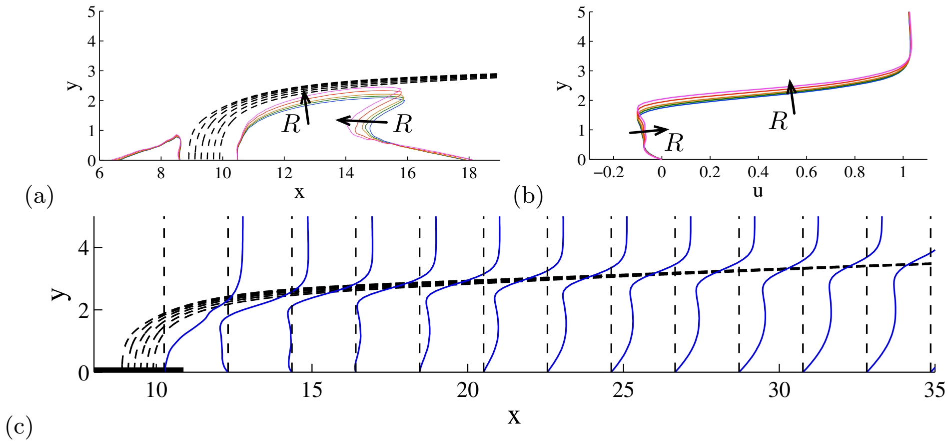

FIGURE 8. (a) The contours of $u = 0$ in the spanwise symmetry plane ($z = 0$) for values of R between 0.65 and 0.8. The streamlines plotted at $R = 0.65$ in the same plane are also shown (dashed lines) to illustrate the position of the reversed flow region with respect to the jet orifice. (b) The 1D profile of the streamwise velocity at $x = 12.3$, again in the spanwise symmetry plane ($z = 0$), is shown for the same range of R. The arrows in (a) and (b) indicate the change of the plotted quantities as R is increased. c) The 1D profile of the streamwise velocity of the steady case at $R = 0.65$ is shown at a number of streamwise stations, again in the spanwise symmetry plane, indicating regions of strong shear in the shear layer due to the backflow near the wall. The jet nozzle is indicated by the thick line centered at $x = 9.375$.

example, for a 2D weakly non-parallel flow, the stability of a 1D profile is studied at each streamwise location, and the locus of locations where the 1D profile is unstable is identified. The so-called absolute global frequency, which is the frequency of the limit cycle, may then be extracted using complex analysis (see, for example, Huerre & Rossi (1998)). This method was used to successfully predict the limit cycle frequency for the 2D cylinder by Pier (2002) and Giannetti & Luchini (2007). The stability of 3D flow past a sphere was studied by Pier (2008), and a pocket of absolute instability was determined, although the frequency of oscillation found by DNS was not predicted correctly. We do not know whether the reasonable success of local methods might extend to the jet in crossflow, which is an even more complex 3D flow. Fortunately, thanks to the significant increase in available computational power in the recent years and the development of appropriate computational methods, we are able to characterize the instability mechanism by utilizing the tools of global stability analysis for 3D flows, which involves no assumptions or simplifications such as those that impose limitations on local methods.

4. Stability analysis

We next study the global stability of the jet in crossflow at $R = 0.675$, i.e., for the case where the first limit cycle is observed as R is increased. Infinitesimally small oscillations of a perturbed steady system about an equilibrium are governed by a linear operator. The main idea of linear stability analysis is to compute the eigenvalues and eigenvectors of the linear operator in order to study the dynamics of the perturbation. For fluid flows, the linear dynamics of the perturbation is given by the linearized Navier-Stokes equation:

$$\frac{\partial \mathbf{u}}{\partial t} = -(\mathbf{U}\cdot\nabla)\mathbf{u} - (\mathbf{u}\cdot\nabla)U - \nabla p + Re^{-1}\nabla^2\mathbf{u} + f(x)\mathbf{u} \tag{4.1}$$

$$\nabla\cdot\mathbf{u} = 0, \tag{4.2}$$

where the full solution is defined as $\mathbf{u}' = \mathbf{U}+\mathbf{u}$, where $\mathbf{u}' = (u', v', w')$ are the streamwise, wall-normal and spanwise components of the full velocity field, and $\mathbf{u} = (u, v, w)$ are the components of the perturbation field†. The field $\mathbf{U} = (U, V, W)$ is a steady-state (equilibrium) solution about which the perturbation $\mathbf{u}$ evolves. We note that $\mathbf{U}$, which is also known as the *base flow*, is typically different from the mean flow. In the case of unsteady flows, this solution is unphysical and can only be obtained numerically. The forcing term $f(x)$, also known as a *fringe*, enforces the periodic boundary conditions in the streamwise direction in our numerical method (Chevalier *et al.* 2007). Equation 4.2 can be re-written as:

$$\dot{\mathbf{u}} = \mathbf{A}\mathbf{u}, \tag{4.3}$$

where the operator $\mathbf{A}$ is the linearized Navier-Stokes operator.

The spatial structure of the eigenvectors of $\mathbf{A}$, which are also known as global eigenmodes, reveals the characteristic flow structures of the perturbation. The real and imaginary parts of the complex eigenvalues of $\mathbf{A}$, defined as $\lambda = \sigma \pm i\omega$, correspond respectively to the temporal growth rate and oscillation frequency of the eigenvectors. The first stability analysis for a jet in crossflow was performed by Bagheri *et al.* (2009*b*) at $R = 3$, and we refer the reader to that work for more details on the numerical procedure. It was found that the flow contains unstable modes with different spatial structures and symmetries, which are summarized in table 1. Here we perform the same analysis at low values of R, the DNS of which was studied in Sec. 3, and we take a closer look at the dynamics near the first instability.

Due to the three-dimensional nature of the flow, solving the eigenvalue problem can be achieved only using a time-stepper-based method, since the matrix $\mathbf{A}$ cannot be stored in computer memory for the, as it would require about 4 Pbytes of storage for our grid resolution. The eigenmodes were computed using the Implicitly Restarted Arnoldi Method (IRAM, Lehoucq *et al.* 1998), using the linearized DNS timestepper for the SIMSON solver described by Bagheri *et al.* (2009*b*). The parallelization of the timestepper was modified with respect to that of Bagheri *et al.* (2009*b*) in order to enable the use of a larger number of CPUs as described in Li (2009). The boundary conditions on top of the computational box were Dirichlet boundary conditions ($u = v = w = 0$). We note that for the stability analysis these are conditions on the perturbation, which obeys the linearized Navier-Stokes equations, and not on the full nonlinear flow. It was carefully tested that the box is high enough for an evolution of a linear perturbation to be virtually identical when using Dirichlet or Neumann boundary conditions on top of the box. The convergence of the most unstable modes was tested through runs of the IRAM at different tolerances, and it was found to be excellent.

4.1. *Base flow*

The base flows were obtained in each case using Selective Frequency Damping (SFD). For details of this method, which damps the oscillations of the unsteady part of the solution using a temporal low-pass filter, see Åkervik *et al.* (2006). This is achieved by adding a forcing term to the nonlinear Navier-Stokes equations of the form

$$-\chi(\mathbf{u}' - \hat{\mathbf{u}}'), \tag{4.4}$$

where $\hat{\mathbf{u}}'$ is a temporally low-pass-filtered state given by

$$\partial_t \hat{\mathbf{u}}' = (\mathbf{u}' - \hat{\mathbf{u}}')/\Delta. \tag{4.5}$$

† The perturbation field is often denoted with a prime, while the full solution typically has no primes. Here we will be dealing mostly with the perturbation field, so we choose to drop the prime on it.

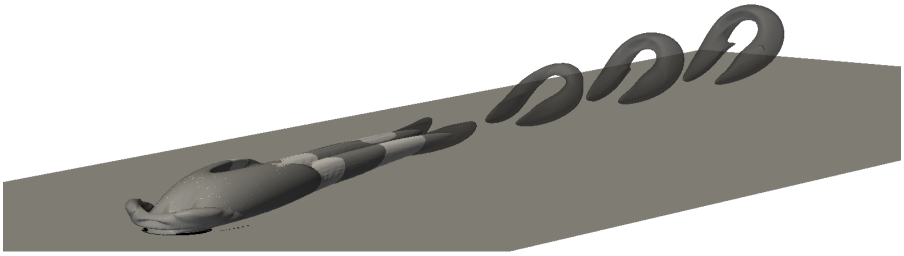

FIGURE 9. The same isosurface of λ_2 for the same snapshot of Fig. 6a, here plotted in dark gray and overlayed on top of the isosurface of λ_2 for the base flow (white), showing that the two flow fields are nearly identical in the near-field of the jet.

Typical values used for the two SFD parameters were $\Delta = 2$ and χ between 0.6 and 1. The convergence of the base flow can have a significant effect on the results of the stability calculations, and in particular on the growth rates of the eigenmodes. It was found that the frequencies obtained from preliminary calculations using unconverged base flows were close to the correct frequencies obtained with properly converged base flows, but the corresponding growth rates were quite different, and the first bifurcation was not predicted correctly. The convergence of the base flows used in the computations was checked by computing the modes using both the final snapshot of a SFD simulation as the base flow, and a snapshot from a few hundred time units earlier, and verifying that the eigenvalue variation is negligible.

The converged base flow for the first supercritical case, $R = 0.675$, is shown in white in Fig. 9 together with a snapshot of the limit cycle (gray). This base flow is very close to the steady solution at $R = 0.65$ shown in Fig. 5, and has the same flow features: a weak CVP, the stable horseshoe vortex, the reversed flow regions upstream of the jet and behind it, as well as the windward and leeward shear layers that coalesce into an 'envelope' as evident from the λ_2 isosurface. In Fig. 9a, we plot the same isosurface of λ_2 for the base flow and a snapshot of the limit cycle, showing that the two fields are almost identical in the near-field of the jet, but further downstream, the hairpin vortices are present in the DNS snapshot, but not in the base flow. This figure demonstrates that there is little or no oscillation of the nonlinear solution in the region immediately downstream of the jet. As argued in Section 3.3, the global shedding frequency is imposed in that region of the flow, and we may thus expect linear stability analysis around this base flow to predict the frequency well, since the base flow is close to the limit cycle mean in that region.

It is also of interest to compare the base flow to the mean flow of the DNS. The base flow, although not a flow field occurring in practice, is the unstable solution whose instability leads to the limit cycle, and which is thus essential to the flow dynamics. On the other hand, the nonlinear limit cycle can be decomposed into a mean flow and a part of the solution that oscillates about it, but the mean flow does not govern the dynamics. The difference between the mean velocity field of the DNS and the base flow has been defined as a *shift mode* by Noack *et al.* (2003). Insight about the relevance of a linear stability analysis and its potential to accurately predict the dynamics of the nonlinear flow may thus be obtained by studying the difference between the mean flow and the base flow.

Fig. 10(a) shows the boundary of the separation region and the streamlines that illustrate the jet trajectory from Fig. 8(a), plotted both for the mean flow and the base flow.

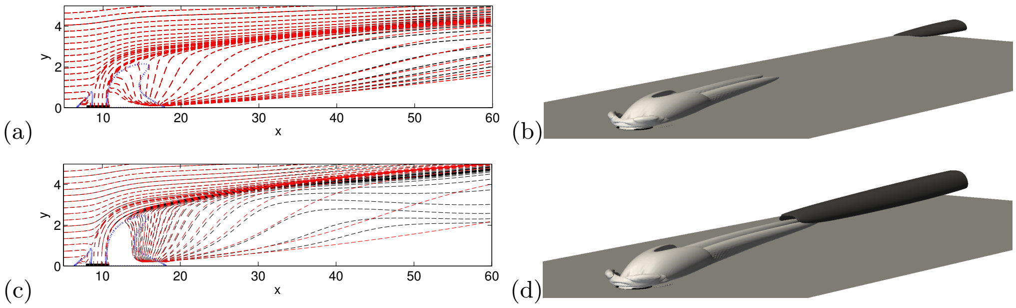

FIGURE 10. (a) Streamlines for the mean flow (black lines) and base flow (red lines) for the mid-plane at $R = 0.675$. The blue contour indicates the border of the separation region (overlapping for the two fields). (b) An isocontour of the streamwise velocity component of the 'shift mode' at $u = 0.05$ (dark grey), shown together with the same isosurface of λ_2 of the base flow from Fig. 9(a). The equivalent plots for $R = 0.8$ are shown in (c) and (d). In (c), the blue contour again indicates the border of the separation region, which is almost perfectly overlapping for the two fields. In (d), the isocontour level for the streamwise velocity of the shift mode (dark grey) is now 0.15, indicating the significantly larger difference between the mean flow and the base flow.

The two fields are identical in the near-field of the jet, and there is only a slight difference in the streamlines downstream. The shift mode is visualized in 3D in Fig. 10(b), together with the same isosurface of λ_2 of the base flow as in Fig. 10(a). The values shown are half of the minimum and half of the maximum of the streamwise velocity component of the shift mode. The maximum magnitude of the shift mode is 0.07, compared to the maximum magnitude of streamwise velocity in the mean flow, which is 1.04, i.e., about 6%. Figures 10(a) and 10(b) indicate that the difference between the unstable steady-state solution and the actual mean flow from the DNS is very small, and moreover, the two are identical in the region where the instability of the shear layer originates.

On the other hand, the streamlines are also compared for $R = 0.8$ in Figure 10(c) and the corresponding shift mode is shown in 10(d). Here the maximum magnitude of the shift mode is 0.26, compared to the maximum magnitude of streamwise velocity in the mean flow, which is 1.04 (just slightly different from that of the mean flow at $R = 0.675$), i.e., about 25%. In addition, the streamlines of the mean flow and base flow look much more different than for $R = 0.675$. However, the boundary of the separation region is still almost identical for the two fields (not shown for the mean flow in order not to clutter the figure), and the streamlines in the near field are almost identical as well.

Based on the comparison in Figure 10, we may expect linear stability analysis to provide a reasonably accurate picture not only of the initial evolution of the perturbation, but also of the limit cycle, at least in terms of the frequency of the self-sustained oscillation, since in the region where we believe that the global frequency is imposed (recall Sec. 3.3), the base flow matches the mean flow very well. We also note that stability analysis about a mean flow has been found to be successful in the case of a cylinder (Barkley 2006). However, it was found by Sipp & Lebedev (2007) that, although the frequency of shedding behind a cylinder may be predicted using a linear stability analysis about a mean flow, such an analysis is not successful in the case of an open cavity flow. It remains to be seen whether a stability analysis based on the mean flow would predict correctly the dynamics of the jet in crossflow. If this were the case, this would be useful since the unstable steady states that we use in the present analysis can be obtained only in numerical computations. On the other hand, mean flow measurements of unsteady jets encountered in practice may be obtained in experiments.

Table 2. Comparison of the frequency of saturated oscillation measured from the DNS runs and the frequency of the most unstable eigenmode for different values of R.

R	ω (DNS)	ω (Arnoldi)	% difference
0.675	0.4979	0.4946	0.7
0.7	0.5084	0.4973	2.2
0.75	0.5206	0.5029	3.4
0.8	0.5306	0.5089	4.1

4.2. *Global eigenmodes*

The global eigenmodes were computed for several values of R, and the resulting eigenvalue spectra are displayed in Fig. 11. The curves show a branch of symmetric eigenmodes that become unstable as R is increased, with a very small change in frequency compared to the increase in the growth rate. The frequency of the most unstable mode for each R is very close to the frequency of the limit cycle observed in the corresponding DNS runs discussed in Sec. 3. The unstable eigenmode at $R = 0.675$, as well as the several eigenmodes with highest growth rates, are symmetric with respect to the spanwise direction. This is in contrast to the $R = 3$ case of Bagheri *et al.* (2009*b*), where the mode with the highest growth rate was found to be anti-symmetric. Anti-symmetric modes have also been found in preliminary calculations, but they are much more stable than the symmetric ones. These modes are not present in the spectra that we show here, since we only compute a few unstable modes at each R due to the high computational expense of the IRAM. We also note that at least one mode corresponding to a purely real eigenvalue (i.e., zero frequency) is observed at each R. These modes are denoted by circles in Fig. 11 and are symmetric and elongated, without the wave-like structure of the oscillating modes.

The real part of the spanwise vorticity component of the unstable eigenmode at $R = 0.675$ is shown in Fig. 12(a). The growth rate is $\sigma = 0.00094$, and the frequency of oscillation is $\omega = 0.4946$, corresponding to a Strouhal number of 0.350, which is very close to the Strouhal number observed from the DNS ($St = 0.353$). The eigenmode has its highest magnitude downstream towards the outflow region of the domain, indicating that it corresponds to a structure that grows in space as it develops on top of the CVP. The alternating positive and negative isocoutours indicate that it is a wave-like structure with a clearly distinguishable spatial wavenumber.

These structures correspond to the same kind of hairpin vortices as those seen in the DNS run; however their spatial wavenumber is different, which is due to the difference in the convection speed between the mean flow and the base flow, which is well illustrated by the shift mode shown in Fig. 10.

In contrast to the symmetric modes shown by Schlatter *et al.* (2010) for the jet at $R = 3$, whose spatial support is typically localized around the initial upstream part of the CVP, the modes shown here have spatial support over the entire streamwise length of the shear layer, and their magnitude is the largest near the box outflow.

The shape of the modes shown in Fig. 12 may be regarded as further evidence in support of an absolute instability of the separation region which is followed by a convectively

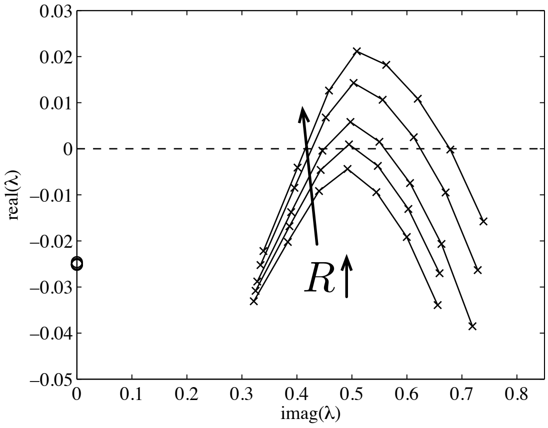

FIGURE 11. Eigenvalue spectra for the jet in crossflow for different values of R. The arrow indicates the change in the spectra as R is increased from $R = 0.65$ to $R = 0.8$.

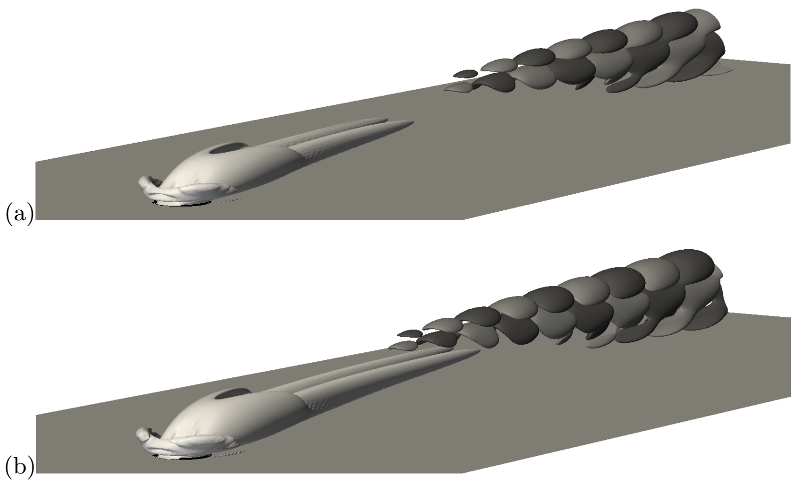

FIGURE 12. (a) The real part of the unstable eigenmode for $R = 0.675$. Isosurfaces of positive (dark grey) and negative (light grey) spanwise vorticity are shown at 19% of the minimum/maximum value respectively. The white isosurface is the base flow, showing $\lambda_2 = -0.0085$. (b) Same as (a) for $R = 0.8$, now showing 11% of minimum/maximum value of the spanwise vorticity. Note the slightly longer CVP in the base flow λ_2 isosurface.

unstable amplifying region downstream. The location of the maximum of the unstable eigenvector is far downstream of the separation region, at the end of the computational domain. This is in accordance with the observation by Huerre & Monkewitz (1990) that the region where the local absolute instability is strongest in a spatially developing flow occurs far upstream of the maximum of the unstable mode. The shear layer thus acts as an amplifier, and the perturbations grow as they convect downstream and the shedding of the shear layer vortices becomes stronger.

We also observe that the frequency of the most unstable mode is a good estimate of the limit-cycle frequency even when multiple unstable modes are present at higher R. Table 2 compares the frequencies obtained from spectral analysis of the probes from the DNS runs and the frequencies of the most unstable eigenmode at a number of values of R. As may be expected, the discrepancy between the two frequencies increases as R is increased, although at $R = 0.8$ the difference is still fairly small — 4.1%. Also, while both columns indicate an increase in frequency with increasing R, the change is much slower for the frequencies of the eigenmodes; while the increase in the frequency in the DNS runs is 6.2% between $R = 0.675$ and $R = 0.8$, it is only 2.8% for the linear stability analysis. This difference is correlated with the increasing deviation of the mean flow from the base flow demonstrated earlier, meaning that the oscillations in the DNS are about a flow which is now different from the steady-state solution on which the linear analysis is based. Nevertheless, the frequency of the limit cycle and the frequency associated with the most unstable eigenmode are still quite close for $R = 0.8$. The most unstable eigenmode at $R = 0.8$ is shown in Fig. 12(b) and it is qualitatively very similar to the one at $R = 0.675$.

During the transient, multiple frequencies are present in the flow, which is apparent from characteristic beating signatures, as shown in Fig. 7(b), but eventually the frequency corresponding to the most unstable mode is the only one remaining, i.e., the flow has 'locked on' to that frequency. We note that the evolution of nonlinear DNS runs which correspond to values of R where multiple unstable modes were found was not significantly qualitatively different than runs where there was only a single unstable mode, or the flow was stable (except, of course, the nonlinear saturation in the latter case). The beats observed in many runs are not only due to unstable modes, but also due to the presence of slowly decaying stable modes with similar spatial structure as the unstable ones.

4.3. *Comparison of stability results with the DNS*

We next examine more closely the correspondence between the results of the linear stability analysis and the dynamics observed in the DNS. The match between the frequency of oscillation in the DNS and the frequency of the most unstable mode at $R = 0.675$ is excellent, and it remains very close up to $R = 0.8$. While linear stability analysis is certainly expected to capture well the initial evolution of a perturbation, we do not necessarily expect it to capture well the limit cycle, yet here that is the case in terms of the frequency. On the other hand, the shape and spatial frequency of the hairpin vortices in the DNS are not matched by the linear eigenmode, which is what we focus on next.

A simulation at $R = 0.8$ was initiated with the base flow as initial condition, and therefore the excitation of the unstable modes was only due to the numerical noise. It was observed that the amplitude of the solution at the probe locations slowly increases until the full limit cycle amplitude is reached. As shown above, four unstable modes are present in this case, but after initial linear interaction among those modes, the solution continues to grow at exactly the growth rate of the most unstable mode, and the frequency was found to match the one computed from the stability analysis. We note that the simulation takes more than a thousand non-dimensional time units to reach saturation, confirming that the base flow for this case is very well converged.

In Figure 13 (a) the wall-normal velocity for $R = 0.8$ at the location $(60.0, 4.1, 1.5)$ is plotted, and Fig. 13 (b) shows the corresponding PSD during initial stages of appreciable growth, where both the frequency and the growth rate of the mode are exactly as predicted by the linear stability analysis. Figures 13 (c) contains the same comparison for a later time window that includes nonlinear saturation, and the corresponding PSD is plotted in Fig. 13 (d). The PSD now shows additional peaks corresponding to harmonics, but the fundamental frequency is also different by a few percent. A component at zero frequency is also visible, indicating that the mean flow itself is evolving during this period.

It may be concluded that the linear stability analysis is able to predict the initial growth rate of the perturbation, as well as its frequency both initially and for the limit

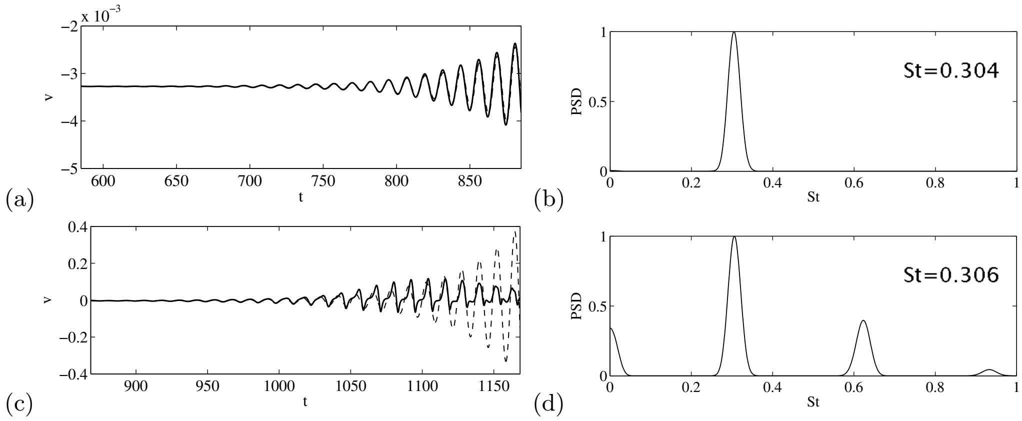

FIGURE 13. (a) Wall-normal velocity $(60.0, 4.1, 1.5)$ (black line) and the linear evolution of a signal predicted by the stability analysis (dashed line) for the period $t = 585 - 885$. The corresponding PSD is shown in (b). The same is shown for the period $t = 868 - 1168$ in (c) and (d). Note the change in scale on the y-axis between the (a) and (c).

cycle. The ability to predict the global frequency of oscillation using the results of the linear stability analysis appears to be due to the fact that the global frequency is imposed in the near-field region of the jet, where the base flow and the mean flow are very close. The tools of stability analysis allow us to further examine the importance of this region for the global dynamics in the next section.

4.4. *Adjoint global modes and 'wavemaker'*

In order to study the dynamics of the instability of the jet in crossflow in greater detail, we have also computed the adjoint global eigenmodes for values of R near the first bifurcation. The concept of adjoint originates from optimization, and adjoint-based methods have been used successfully in flow control and stability. The adjoint operator of A has the property that:

$$\langle Ax, y \rangle = \left\langle x, A^{+}y \right\rangle, \tag{4.6}$$

where the $\langle \cdot, \cdot \rangle$ denotes the appropriate inner product for the flow domain. We present, to the best of our knowledge, the first computation of fully three-dimensional adjoint global eigenmodes, and certainly the first such computation for the jet in crossflow. The adjoint modes are useful for sensitivity analysis of the flow - it can be shown (Giannetti & Luchini 2007) that the magnitude of the adjoint eigenmode indicates the regions in the flow that are receptive to momentum forcing, i.e., if a control device were introduced at that point in the flow, the response would be very strong. The derivation of the adjoint linear Navier-Stokes equations for the boundary layer, which have been used in this work as well, may be found in Bagheri *et al.* (2009*a*). These equations have a form very similar to that of the linearized Navier-Stokes equations defined in Eq. 4.2 due to the use of Dirichlet boundary conditions for the perturbation on the top of the computational domain. Since the adjoint equations are very similar to the linearized Navier-Stokes equations, a modified version of the same SIMSON timestepper is used, and the eigenvalue problem is solved using the same IRAM code used for the direct eigenmodes. Since the eigenvalues of the continuous linearized operator A and its adjoint A^{+} are the same, comparing the eigenvalues of the two operators obtained using IRAM is an important check of the computations. We found that for the most unstable direct-adjoint eigenmode pair, the error between the two computations was typically on the

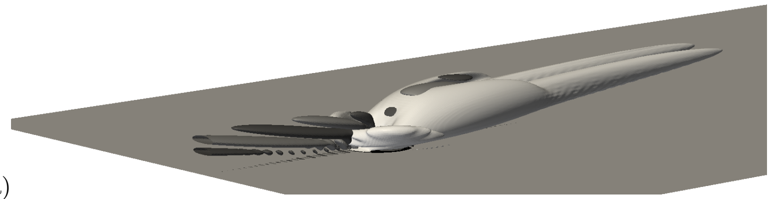

(a)

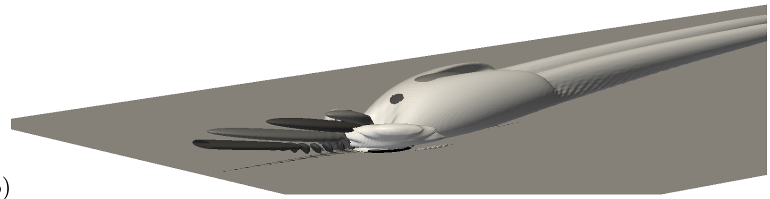

(b)

FIGURE 14. The real part of the unstable adjoint eigenmode for $R = 0.675$ (a) and $R = 0.8$ (b). Isosurfaces of positive (dark grey) and negative (light grey) spanwise vorticity are shown. The white isosurface is the base flow, showing $\lambda_2 = -0.0085$ in both cases.

order of 10^{-8} for the growth rate (real part of the eigenvalue) and on the order of 10^{-10} for the frequency (imaginary part of the eigenvalue), which provided a verification of our implementation of the continuous adjoint in the SIMSON-based IRAM timestepper.

Figure 14 shows the leading adjoint eigenmodes for $R = 0.675$ and $R = 0.8$. The modes consist of upstream traveling structures that are characteristic for adjoint simulations in spatially developing flows. We note that the adjoint modes are localized both in the region of the flow upstream of the jet itself and in the downstream shear layer. This indicates that the flow is highly sensitive to forcing in these areas. The region of the flow upstream of the jet orifice indicates that perturbations incoming with the crossflow in or near the spanwise symmetry plane would be amplified by the jet and grow downstream. The region in the shear layer is perhaps of greater interest for us, since the shedding of hairpin vortices observed in the DNS has been connected to the self-sustained oscillation of the shear layer. The adjoint modes now indicate that this region is highly sensitive to forcing, which may be introduced by perturbations in that region of the flow.

The adjoint mode by itself only shows the sensitivity of the flow to volume forcing, but does not provide information on the sensitivity of the growth rate and shedding frequency, i.e., on the complex eigenvalue of the linearized Navier-Stokes operator. However, in combination with the direct global eigenmode, the sensitivity of the eigenvalues of A can be studied, which is much more useful for flow control strategies than simply looking at the receptivity of the flow. The concept of a 'wavemaker' as a region in the flow where the global frequency is imposed was introduced by Chomaz (2005). Physically, this is a region in the flow where the self-sustained oscillation is 'born' from a local absolute instability, and its character in terms of the oscillation frequency and the flow structures is imposed. On the other hand, mathematically, this is a region where the eigenvalue of the linearized operator is highly sensitive to a localized feedback mechanism, that may be introduced by a device that introduces forcing dependent on the local velocity, as shown by Giannetti & Luchini (2007). It has been shown (Chomaz 2005) that the 'wavemaker' may be located simply by computing the overlap of the direct and adjoint global modes. In particular, the magnitude of the eigenvalue drift due to such forcing

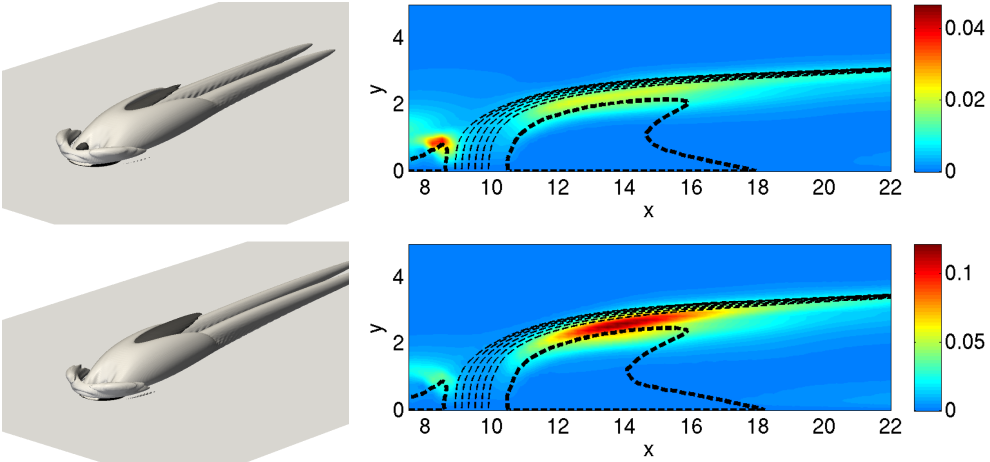

FIGURE 15. The overlap of the direct and adjoint mode, also known as a 'wavemaker', for $R = 0.675$ (top) and $R = 0.8$ (bottom). On the left, an isosurface of each region is visualizes in 3D (black) together with λ_2 isosurfaces of the corresponding base flow. On the right, a cut of the overlaps in the spanwise symmetry plane ($z = 0$) is shown, along with streamlines that illustrate the jet trajectory (thin dashed lines) and the boundary of the backflow region (thick dashed lines).

can be shown (Giannetti & Luchini 2007) to be bounded by the the function

$$\eta(x, y, z) = \frac{\|\hat{\mathbf{q}^+}\|\|\hat{\mathbf{q}}\|}{\int_D \hat{\mathbf{q}^+} \cdot \hat{\mathbf{q}} dS}, \tag{4.7}$$

where we define $\hat{\mathbf{q}}(x, y, z)$ as the global eigenmode, and $\hat{\mathbf{q}^+}(x, y, z)$ as the corresponding adjoint eigenmode†.

The overlap of the leading pair of global and adjoint modes is shown in Fig. 15 for both $R = 0.675$ and $R = 0.8$. The overlap indicates that the linearized operator in this case is highly sensitive to a localized feedback in the downstream shear layer, which is the region that, based on the evidence presented earlier, we have suspected to be the 'wavemaker' from physical reasoning. In addition, we observe a small region of high sensitivity just behind the steady horseshoe vortex. In fact, the magnitude of $\eta(x, y, z)$ is highest in that region for the $R = 0.675$ case. We have not, however, observed any instabilities in the DNS originating upstream of the jet orifice, as described in the previous section. The numerical value of the overlap may be interpreted as the magnitude of a possible eigenvalue drift as a result of an applied perturbation in the given region. This drift is still significant in the downstream shear layer at $R = 0.675$. The overlap of the direct and adjoint mode was also found to have its peaks in the shear layers caused by the border of the reversed flow region in the cylinder in crossflow (Giannetti & Luchini 2007). The fact that the highest value of the overlap shifts to the downstream shear layer for $R = 0.8$ indicates that, as the downstream shear layer becomes stronger, the flow becomes more and more sensitive to shear layer instabilities, which may be expected on physical grounds. On the other hand, since the flow upstream of the jet exit does not change appreciably between the two values of R, the sensitivity in that region remains approximately the same, as can be seen from a comparison of the magnitudes of the upstream peak of the overlap.

† We note that the overlap function was denoted by λ when introduced by Giannetti & Luchini (2007), but here we use η due to our definition of the complex eigenvalue as λ.

We wish to emphasize that care must be taken when studying sensitivity using a linear stability analysis, since the results need to be converged with respect to the computational box size, resolution and boundary conditions. While a study of box independence such as the one undertaken for example by Giannetti & Luchini (2007) is not feasible for our current setup, preliminary studies conducted earlier using a very similar configuration in a shorter box (total streamwise length $L_x = 50$, including the fringe region, as opposed to $L_x = 75$, as used in all other simulations) indicate that the physically relevant 'wavemaker' region is indeed captured correctly in our computations. In the shorter box, we observed that the first bifurcation occurs at about $R = 0.8$ (as opposed to $R = 0.675$ for the longer box), but the frequency of the most unstable eigenmode in the two cases is very close ($St = 0.294$ for the short box and $St = 0.304$ for the long box). The growth rate, however, is quite different — 0.021 for the long box compared to 0.006 for the short box. Nevertheless, the overlap of the first global eigenmode and the corresponding adjoint eigenmode is still located in the same location. We show the overlap regions for the two computational boxes in Fig. 16. A region of overlap near the wall in the far field is observed in both cases. This region has its peak at the beginning of the fringe used to enforce the periodic boundary conditions in the streamwise direction, and it was found that some of the adjoint solution is re-circulated in the upstream direction due to the fringe. This region was therefore determined to be unphysical, especially since it moves downstream and has a lower peak value compared to the peak of the overlap in the shear layer as the box length is increased.

It is interesting to note that the additional region of overlap that we observe in the far field points to the high sensitivity of the stability results to the simulation setup, and in this case the box length in particular. Indeed, changing the box length changes the growth rate of the global eigenmodes, and this is reflected in the observed overlap region. The magnitude of η in the short box near the fringe is approximately 0.02, which is of the same order of magnitude as the difference in the growth rate of the most unstable eigenvalue between the two boxes, which is 0.016, indicating that the sensitivity of our numerical setup is estimated well by the physically spurious overlap region. As expected, as the box length is increased, the relative importance of the additional overlap region is lower, indicating that improved convergence would be achieved either by a much longer computational domain, or a method that does not allow disturbances to enter the flow domain from the outflow in the case of the adjoint simulation.

We also note that, although the maxima of the adjoint modes shown in Fig. 14 were found to be contained within our computational box, the true maximum of the direct mode shown in Figure 12 is likely to be further donwstream than the extent of our longer box. However, based on the findings of works on the cylinder in crossflow (Giannetti & Luchini 2007) and a confined plane wake (Tammisola *et al.* 2011), the modes become more and more elongated as the bifurcation parameter is decreased, and the same appears to be true for the jet in crossflow. On the other hand, as pointed out by Chomaz (2005), capturing the overlap of the modes, or the 'wavemaker', is sufficient for capturing the relevant dynamics of the global eigenmodes.

5. Discussion and conclusions

We have examined the jet in crossflow at low values of the velocity inflow ratio R using direct numerical simulations and a three-dimensional global linear stability analysis. Our findings can be summarized as follows:

(i) The first instability was found to occur at the velocity ratio $R = 0.675$, when a limit cycle characteristic of a Hopf birufcation is established. The DNS computa-

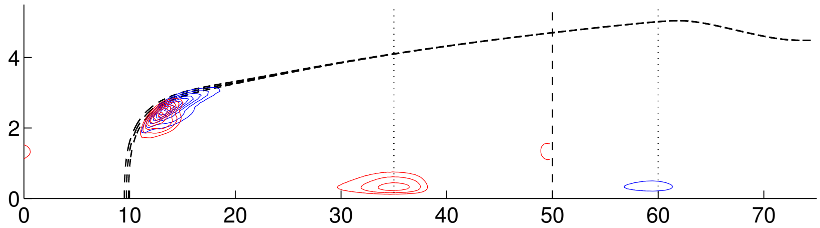

FIGURE 16. A comparison of the overlap of the direct and adjoint global eigenmodes at $R = 0.8$ for a short box (red) and a longer box (blue). The vertical dashed line at $x = 50$ indicates the end of the short box, while the dotted vertical lines at $x = 35$ and $x = 60$ indicate the beginning of the fringe region for the short and long boxes respectively.

tions indicate that a self-sustained oscillation arises in the downstream shear layer and that it may be due to a local absolute instability in the reversed flow region downstream of the jet orifice, which forms because the jet acts as an obstacle to the inflow. The resulting limit-cycle persists at higher values of R, although above $R = 1$ the vortical structures in the flow become more complex. This flow regime will be studied further in the second part of this paper.

(ii) A linear stability analysis has been performed at several values of R around the first bifurcation, and global eigenmodes that correspond to spatially developing shear layer instabilities have been obtained. It is found that the frequency of the limit cycle oscillation is predicted very well, although the shape of the modes obtained is quite different from the shape of the oscillating structures in the DNS. It is also found that the frequency of the limit cycle oscillation can be predicted reasonably well even when the nonlinear flow is further from the bifurcation, i.e., when the base flow and the mean flow are different.

(iii) An analysis of the overlap region of the direct and adjoint eigenmodes, also known as a 'wavemaker', indicates that the shear layer downstream of the jet is indeed a dynamically important region, since the linearized Navier-Stokes equations about the unsteady base flow are most sensitive to perturbations there. It is these perturbations that get amplified downstream, as indicated by the structure of the direct global eigenmodes.

5.1. *Insights about flow dynamics*

The results of Sections 3 and 4 provide the first detailed description of the instability mechanisms that arise in a jet in crossflow based on nonlinear direct numerical simulation and linear global stability analysis. The global stability analysis does not require the assumptions that are necessary for local approaches. Previous experimental and numerical investigations have focused on turbulent cases, or cases at high R where simple instability mechanisms can not be isolated due to the complex interplay of different instabilities. Despite the absence of the jet pipe, the setup allows a clear picture of how the instabilities arise, and when the interaction of different mechanisms becomes complex, leading to the quasi-periodic or chaotic behavior observed in practical jets. We therefore consider this work to be a valuable basis for further studies that will involve the inflow pipe and more realistic inflow profiles and Reynolds numbers.

The global stability analysis reveals that the first instability at critical R is Kelvin-Helmholtz roll-up of the downstream shear layer. Furthermore, we have been able to pinpoint the core of this instability using the overlap between the direct and adjoint modes. The usefulness of the wavemaker analysis lies in the fact that no a priori physical insight into the problem is necessary. While it is of course important to identify intuitively the physical mechanisms that cause instabilities, this may not be straightforward in more complex geometries, or complex flows such as the one considered here. In particular, when there are multiple physical phenomena present in the flow, and competing instability mechanisms that correspond to them, the type of analysis performed here is useful in determining where the first instability arises, and thus potentially useful for control.

An alternative approach to linear stability analysis for supercritical values of R is the study of the periodic orbit using Floquet analysis, and the results of the two methods can be compared to the linear stability analysis. As R increases further above the bifurcation value, it is really the stability of the limit cycle, and not of the stationary base flow, that reveals the true physics of the flow. A sensitivity analysis of the supercritical cylinder wake was performed by Luchini *et al.* (2008), and time evolution of regions sensitive to secondary instabilities in the limit cycle flow was studied. Such an investigation would be useful in evaluating the validity of the linear analysis when multiple frequencies are present in the flow, i.e., it will become clear whether the more complex behavior seen at higher values of R is due to an instability of the limit cycle above the first bifurcation.

5.2. *Insights for flow control and other applications*

Control of jets in crossflow is of great practical importance, and is one of the main motivations for studying the flow. Control studies using pulsing of the jet have been performed by (M'Closkey *et al.* 2002). Determining with certainty if self-sustained oscillations are present and characterizing their dynamics is essential for control of the jet in crossflow, since the effect of sinusoidal forcing may be dramatically changed by the presence of global instabilities, as shown by Megerian *et al.* (2007). Breaking up the self-sustained oscillation, or imposing a different frequency (for example one that would be more desirable for good mixing) will likely require more energy when self-sustained oscillations are present. Studying the jet in crossflow is also important for film cooling applications (see, for example, Jovanović (2006), for a thorough experimental study). Good cooling efficiency corresponds to better mixing, and the mixing has been shown to be related to the coherent structures in the flow (Salewski *et al.* 2008). A key factor, however, is the crossflow inflow at the location of the jet orifice. In Ziefle (2007) it was shown that mixing is much better when the incoming flow is turbulent and unsteady. The strong shedding of hairpin vortices observed for steady inflow is not desirable for cooling applications, as it does not result in a well-mixed coolant layer covering the wall. Since fully turbulent crossflow may not be achieved in some applications, it is important to study the dynamics of these vortices in order to design potential control strategies. We are currently conducting preliminary studies of mixing using passive scalar as tracer.

Further studies of the sensitivity of the eigenvalues to base flow modifications, or to physically realizable forcing instead of an arbitrary modification of the linearized operator have been done by Marquet *et al.* (2008). These new approaches allow the separation of the effects of production and transport terms on the sensitivity of the eigenvalues, as well as the sensitivity of the base flow to a realistic steady force. The latter approach involves the solution of adjoint base flow equations, but provides a more reliable guidance for placement of obstacles in the flow for passive control — it is possible to predict exactly the location of where a small cylinder may be inserted whose presence suppresses vortex shedding past a larger cylinder as in Marquet *et al.* (2008); Pralits *et al.* (2010). The extension of our work to that type of analysis for the jet in crossflow is the subject of further efforts.

5.3. *Further work*

This work has tackled the difficult task of extending methods and analyses typically applied to 2D flows to 3D, which involves very high computational expense. The second part of this paper will focus of the higher on the study of DNS up to $R = 3$, where the multiple instability mechanisms occur simultaneously. Methods used to study this flow regime include Proper Orthogonal Decomposition (POD) and Koopman modes. The latter method has already been applied to the jet in crossflow with success (Rowley *et al.* 2009).

Other possible directions for further work include, but are not limited to: i) a study of the effect of inclusion of the pipe, which would help shed light on the instabilities of this complex flow that have been observed in experiments as well; ii) a study of the effects of crossflow unsteadiness on the observed limit cycle, and iii) a stability analysis using the mean flow instead of an unstable base flow. Finally, careful experiments may be designed in an attempt to confirm our findings. As pointed out by Theofilis (2011), there has been a lack of experiments that would prove or disprove the many recent results in stability and sensitivity analysis.

Acknowledgments

We would like to acknowledge fruitful discussions with Jan Pralits, Simone Camarri, Flavio Giannetti, Outi Tammisola and Luca Brandt at various stages of this work. Computer time was provided by Swedish National Infrastructure for Computing (SNIC) with a generous grant by the Knut and Alice Wallenberg (KAW) Foundation through the Ekman consortium. Some of the simulations were run at the Centre for Parallel Computers (PDC), Royal Institute of Technology (KTH) and the National Supercomputer Centre (NSC), Linköping University in Sweden.

REFERENCES

Åkervik, E., Brandt, L., Henningson, D. S., Hœpffner, J., Marxen, O. & Schlatter, P. 2006 Steady solutions of the Navier-Stokes equations by selective frequency damping. *Physics of Fluids* **18**, 068102.

Acarlar, M. & Smith, C. 1987*a* A study of hairpin vortices in a laminar boundary layer. part 1. hairpin vortices generated by a hemisphere protuberance. *Journal of Fluid Mechanics* **175**, 1–41.

Acarlar, M. & Smith, C. 1987*b* A study of hairpin vortices in a laminar boundary layer. part 2. hairpin vortices generated by fluid injection. *Journal of Fluid Mechanics* **175**, 43–83.

Alves, L. S. de B., Kelly, R. E. & Karagozian, A. R. 2008 Transverse-jet shear-layer instabilities. Part 2. Linear analysis for large jet-to-crossflow velocity ratio. *Journal of Fluid Mechanics* **602**, 383–401.

Alves, L. S. de B., Kelly, R. E. & Karagozian, A. R. 2007 Local stability analysis of an inviscid transverse jet. *Journal of Fluid Mechanics* **581**, 401–418.

Bagheri, S. 2010 Analysis and control of transitional shear flows using global modes. PhD thesis, Royal Institute of Technology.

Bagheri, S., Brandt, L. & Henningson, D. S. 2009*a* Input–output analysis, model reduction and control of the flat-plate boundary layer. *Journal of Fluid Mechanics* **620**, 263–298.

Bagheri, S., Schlatter, P., Schmid, P. J. & Henningson, D. S. 2009*b* Global stability of a jet in cross-flow. *Journal of Fluid Mechanics* **624**, 33–44.

Barkley, D. 2006 Linear analysis of the cylinder wake mean flow. *Europhysics Letters* **75** (5), 750–756.

Chevalier, M., Schlatter, P., Lundbladh, A. & Henningson, D. S. 2007 SIMSON: A pseudo-spectral solver for incompressible boundary layer flows. Technical Report TRITA-MEK 2007:07. KTH Mechanics.

Chomaz, J. 2005 Global instabilities in spatially developing flows: Non-normality and nonlinearity. *Annual Review of Fluid Mechanics* **37**, 357–392.

Coelho, S. L. V. & Hunt, J. C. R. 1989 The dynamics of the near field of strong jets in crossflows. *Journal of Fluid Mechanics* **200**, 95–120.

Cortelezzi, L. & Karagozian, A. R. 2001 On the formation of the counter-rotating vortex pair in transverse jets. *Journal of Fluid Mechanics* **446**, 347–373.

Davitian, J., Getsinger, D., Hendrickson, C. & Karagozian, A. R. 2010 Transition to global instability in transverse-jet shear layers. *Journal of Fluid Mechanics* **661**, 294–315.

Drazin, P. G. & Reid, W. H. 1981 *Hydrodynamic Stability*. Cambridge University Press.

Fric, T. F. & Roshko, A. 1994 Vortical structure in the wake of a transverse jet. *Journal of Fluid Mechanics* **279**, 1–47.

Giannetti, F. & Luchini, P. 2007 Structural sensitivity of the first instability of the cylinder wake. *Journal of Fluid Mechanics* **581**, 167–197.

Grout, R., Gruber, A., Yoo, C. & Chen, J. 2010 Direct numerical simulation of flame stabilization downstream of a transverse fuel jet in cross-flow. *Proceedings of the Combustion Institute* **doi:10.1016/j.proci.2010.06.013**.

Hammond, D. & Redekopp, L. G. 1998 Local and global instability properties of separation bubbles. *European Journal of Mechanics B/Fluids* **17** (2), 145–164.

Huerre, P. & Monkewitz, P. A. 1990 Local and global instabilities in spatially developing flows. *Annual Review of Fluid Mechanics* **22**, 473–537.

Huerre, P. & Rossi, M. 1998 *Hydrodynamics and Nonlinear Instabilities (edited by Godrèche, C. and Manneville, P.)*, chap. 2. Hydrodynamic instabilities in open flows, pp. 81 – 294. Cambridge University Press.

Ilak, M., Schlatter, P., Bagheri, S., Chevalier, M. & Henningson, D. S. 2010 Stability of a jet in crossflow. *arXiv:1010.3766v1* .

Jeong, J. & Hussain, F. 1995 On the identification of a vortex. *Journal of Fluid Mechanics* **285**, 69–94.

Jovanović, M. B. 2006 Film cooling through imperfect holes. PhD thesis, Eindhoven University of Technology.

Karagozian, A. 2010 Transverse jets and their control. *Progress in Energy and Combustion Science* **30**, 1–23.

Kelso, R. M., Lim, T. T. & Perry, A. E. 1996 An experimental study of round jets in cross-flow. *Journal of Fluid Mechanics* **306**, 111–144.

Kelso, R. M. & Smits, A. J. 1995 Horseshoe vortex systems resulting from the interaction between a laminar boundary layer and a transverse jet. *Physics of Fluids* **7** (1).

Lehoucq, R. B., Sorensen, D. C. & Yang, C. 1998 *ARPACK Users' Guide*. Society for Industrial and Applied Mathematics.

Li, Q. 2009 Simulations of turbulent boundary layers with heat transfer. Licentiate Thesis in Mechanics, TRITA-MEK 2009:14.

Lim, T. T., New, T. H. & Luo, S. C. 2001 On the development of large-scale structures of a jet normal to a cross flow. *Physics of Fluids* **13** (3), 770–775.

Luchini, P., Giannetti, F. & Pralits, J. O. 2008 Structural sensitivity of linear and nonlinear global modes. AIAA-2008-4227.

Marquet, O., Sipp, D. & Jacquin, L. 2008 Sensitivity analysis and passive control of cylinder flow. *Journal of Fluid Mechanics* **615**, 221–252.

M'Closkey, R. T., King, J. M., Cortelezzi, L. & Karagozian, A. 2002 The actively controlled jet in crossflow. *Journal of Fluid Mechanics* **452**.

Megerian, S., Davitian, J., Alves, L. S. de B. & Karagozian, A. R. 2007 Transverse-jet shear-layer instabilities. Part 1. Experimental studies. *Journal of Fluid Mechanics* **593**, 93 – 129.

Muldoon, F. & Acharya, S. 2010 Direct numerical simulation of pulsed jets-in-crossflow. *Computers & Fluids* **39**, 1745–1773.

Muppidi, S. & Mahesh, K. 2005 Study of trajectories of jets in crossflow using direct numerical simulations. *Journal of Fluid Mechanics* **530**, 81 – 100.

Muppidi, S. & Mahesh, K. 2007 Direct numerical simulation of round turbulent jets in crossflow. *Journal of Fluid Mechanics* **574**, 59 – 84.

Noack, B., Afanasiev, K., Morzyński, M., Tadmor, G. & Thiele, F. 2003 A hierarchy of low-dimensional models for the transient and post-transient cylinder wake. *Journal of Fluid Mechanics* **497**, 335–363.

Perry, A. E. & Lim, T. T. 1978 Coherent structures in coflowing jets and wakes. *Journal of Fluid Mechanics* **88**, 451–463.

Pier, B. 2002 On the frequency selection of finite-amplitude vortex shedding in the cylinder wake. *Journal of Fluid Mechanics* **458**, 407 – 417.

Pier, B. 2008 Local and global instabilities in the wake of a sphere. *Journal of Fluid Mechanics* **603**, 39–61.

Pralits, J. O., Brandt, L. & Giannetti, F. 2010 Instability and sensitivity of the flow around a rotating circular cylinder. *Journal of Fluid Mechanics* **650**, 513–536.

Rowley, C. W., Mezić, I., Bagheri, S., Schlatter, P. & Henningson, D. S. 2009 Spectral analysis of nonlinear flows. *Journal of Fluid Mechanics* **641**, 115–127.

Salewski, M., Stankovic, D. & Fuchs, L. 2008 Mixing in circular and non-circular jets in crossflow. *Flow, Turbulence and Combustion* **80**, 255 –283.

Schlatter, P., Bagheri, S. & Henningson, D. S. 2010 Self-sustained global oscillations of a jet in crossflow. *Theoretical and Computational Fluid Dynamics* **doi: 10.1007/s00162-010-0199-1**.

Schmid, P. J. 2007 Nonmodal stability theory. *Annual Review of Fluid Mechanics* **39**, 129–162.

Schmid, P. J. & Henningson, D. S. 2001 *Stability and Transition in Shear Flows*, *Applied Mathematical Sciences*, vol. 142. Springer-Verlag.

Sipp, D. & Lebedev, A. 2007 Global stability of base and mean flows: a general approach and its applications to cylinder and open cavity flows. *Journal of Fluid Mechanics* **593**, 333–358.

Smith, S. H. & Mungal, M. G. 1998 Mixing, structure and scaling of the jet in crossflow. *Journal of Fluid Mechanics* **357**, 83–122.

Tammisola, O., Lundell, F., Schlatter, P., Wehrfritz, A. & Söderberg, L. D. 2011 Global linear and nonlinear stability of viscous confined plane wakes with co-flow. *Journal of Fluid Mechanics* **doi:10.1017/jfm.2011.24**.

Theofilis, V. 2011 Global linear instability. *Annual Review of Fluid Mechanics* **43**, 319 – 352.

Yuan, L. L., Street, R. L. & Ferziger, J. H. 1999 Large-eddy simulations of a round jet in crossflow. *Journal of Fluid Mechanics* **379**, 71 – 104.

Ziefle, J. 2007 Large-eddy simulation of complex massively-separated turbulent flows. PhD thesis, ETH Zurich, Diss. No. 17846.